Analytical Methods

ROYAL SOCIETY OF CHEMISTRY

PAPER

View Article Online
View Journal | View Issue

Cite this: *Anal. Methods*, 2021, **13**, 1121

Carbon dots derived from *Fusobacterium nucleatum* for intracellular determination of Fe^{3+} and bioimaging both *in vitro* and *in vivo*

Lijuan Liu, †[a] Shengting Zhang,†[b] Xiaodan Zheng,[a] Hongmei Li,[c] Qi Chen,[d] Kunhao Qin,[e] Yafang Ding[a] and Yunlin Wei *[a]

Received 5th January 2021
Accepted 27th January 2021

DOI: 10.1039/d1ay00020a

rsc.li/methods

Intracellular Fe^{3+} amount is one of the critical determinants of human health. The development of simple and effective probes for the quantitative detection of Fe^{3+} *in vivo* is of great significance for the early diagnosis of disease or disorder associated with iron deficiency or overload. In this study, remarkable carbon dots, which can serve as a biosensor for efficient intracellular Fe^{3+} detection, were synthesized by hydrothermal carbonization of *Fusobacterium nucleatum*, an anaerobic bacterium. The achieved *F. nucleatum*-carbon dots (Fn-CDs) possessed the features of strong fluorescence, high stability and excellent biocompatibility. The obtained Fn-CDs could easily internalize into both plant cells and human cells with excellent ability for cell tracking and biomedical labeling. The fluorescence of Fn-CDs could still remain for another 24 hours after penetrating into cells. Furthermore, the fluorescent Fn-CDs were very sensitive to the presence of Fe^{3+} ions even in cells, exhibiting great promising applications in *in vivo* detection of Fe^{3+} ions. In addition, the Fn-CDs posed no harm to the mice, being circulated and excreted within a short time, making the Fn-CDs an excellent candidate for bioimaging and biosensing *in vivo*.

1. Introduction

Fluorescent carbon dots (CDs), as a new class of nanomaterials, have aroused immense scientific interest in the last decade due to their advantages of nontoxicity and easy fabrication over conventional semiconductor quantum dots.[1] CDs have displayed extensive application in drug delivery,[2–4] bioimaging,[5,6] pollutant and metal ion detection[7,8] and so on. Natural sources have been preferably exploited to synthesize CDs owing to their low cost, abundance and eco-friendly nature.[9] Continuous efforts have been made to employ a suitable green source to successfully fabricate CDs. Recently, many natural sources have been utilized as the carbon source for the preparation of CDs. Shi *et al.* prepared fluorescent CDs through hydrothermal treatment of corn stalk with an absolute quantum yield of 7.6%.[10] Naik *et al.* achieved CDs derived from leaves of *Andrographis paniculata*, which can serve as a bioimaging agent for cancer cells.[11] Wei *et al.* synthesized CDs from *Gynostemma*, which can be applied as an antioxidant and a biosensor.[9] Soybean-derived CDs were achieved by Wang *et al.* through hydrothermal carbonization and laser ablation in NH_4OH solution.[12] Huang *et al.* reported the synthesis of CDs for the detection of Fe^{3+} and adenosine triphosphate from *Bauhinia* flower.[13] Dehvari *et al.* prepared CDs from crab shells with improved optical properties under conjugation with folic acid.[14] Atchudan *et al.* synthesized CDs from banana peel waste with the function of bioimaging *in vivo*.[15] Sun *et al.* reported the synthesis of CDs through hydrothermal treatment of sodium citrate dihydrate and urea on which DOX was conjugated for drug delivery.[16] Kailasa *et al.* reported that three fluorescent color CDs (blue, green, and yellow) were synthesized from tomato with H_2SO_4 and H_3PO_4 as oxidizing agents.[17] Although the above methods using natural materials as a carbon source to synthesize CDs are feasible and cost-effective, providing the resultant CDs with abundant chemical groups on their surface,[18] it can be noticed that these methods suffer disadvantages of insufficient quantum yields and limited applications or involvement of strong acid or alkali.[10] On the other hand, more efforts have been focused on the approaches to especially achieve CDs with enhanced optical properties for bioimaging applications.[19] As we have reported previously,[20] most of the bacteria, including aerobes and anaerobes, playing a critical part in carbon and nitrogen cycles in the ecosystems, have not achieved enough attention. Compared with the huge

[a]*Faculty of Life Science and Technology, Kunming University of Science and Technology, Kunming 650500, China. E-mail: weiyunlin18@163.com*

[b]*Department of Education, Yunnan Minzu University, Kunming 650500, China*

[c]*State Key Laboratory of Phytochemistry and Plant Resources in West China, Kunming Institute of Botany, Chinese Academy of Sciences, Kunming, 650201, China*

[d]*Department of Hematology, The Second People's Hospital of Yunnan Province, The Affiliated Hospital of Yunnan University, Kunming, 650021, China*

[e]*Shenzhen Institute of Respiratory Diseases, The Second Clinical Medical College, Jinan University (Shenzhen People's Hospital), Shenzhen 518020, China*

† These authors have contributed equally to this work.

number of bacteria, the number that have been applied as a precursor for the synthesis of CDs is negligible.

As an important element required by all the organisms, iron is involved in various critical physiological and pathological processes including cellular metabolism, survival and proliferation.[21] The total amount of iron an adult human contains is around 3–5 g,[22] of which more than 80% exist in red blood cells. Many chronic diseases and disorders, such as anemia, are triggered by iron deficiency or overload; it has also been reported that iron toxicity leads to cell damage. Therefore, appropriate intake and storage of iron are critical to the health of human beings. Most current iron detection approaches, including the use of organic dyes, have the disadvantages of high cost, time consumption and low photostability.[23,24] Thus, developing simple and effective probes for the quantitative detection of Fe^{3+} in cells is of great importance and urgently demanded.

Herein, in this work, *F. nucleatum*, a Gram-negative anaerobe, was first employed as a starting material to synthesize CDs through a simple hydrothermal approach without addition of heteroatoms or further surface passivation. The prepared Fn-CDs were selectively sensitive to the presence of Fe^{3+} and could serve as an efficient fluorescent probe for the quantitative determination of Fe^{3+} with the detection limit of 0.82 μM. After penetrating into cells, their FL intensity remained at least for 48 hours and could be quenched after the addition of Fe^{3+}, indicating that Fn-CDs hold the remarkable promising application as a sensing probe for *in vivo* detection of Fe^{3+}. In addition, the cytotoxicity to HeLa cells showed that the resultant Fn-CDs have negligible cytotoxicity, indicating their great potential in biomedical applications with low toxicity and excellent biocompatibility. To our delight, the *in vivo* bioimaging in mice showed that the achieved Fn-CDs could be carried to the lung and heart through blood circulation and could be excreted within 24 hours, demonstrating the potential applicability of Fn-CDs in bioimaging *in vivo*. Compared with previously reported CDs, the Fn-CDs exhibited distinct properties with multiple functions, overcoming the major drawback of limitation in applications which the CDs normally suffer while using natural materials as precursors.

F. nucleatum contributes greatly to the pathogenesis of periodontal disease, also being responsible for the occurrence of various tumors including oral cancer.[25] The method of synthesis of CDs from *F. nucleatum* provided an alternative approach to eliminate the harmfulness of the pathogenic bacterium and convert it to a useful material. There are a great number of bacteria on the earth, providing with ample carbon sources to fabricate CDs. Therefore, the synthesis of carbon dots from bacteria is easily available and sustainable.

2. Experimental section

2.1 Materials

F. nucleatum cells were provided by Guangdong Microbial Culture Collection Center (GDMCC, China). Brain heart infusion (BHI) medium was purchased from Solarbio Life Science (Beijing, China). 2.5 L round bottom vertical anaerobic culture bag and 2.5 L Anaero Packs were obtained from Mitsubishi Gas Chemical Co., Inc. (Mitsubishi, Japan). All reagents and chemicals were of analytical grade and used without further purification. Reagents $FeCl_3$, $FeSO_4$, $PbCl_2$, $CoCl_2$, $BaCl_2$, $NiCl_2$, $ZnSO_4$, KCl, $MnCl_2$, LiCl, $CaCl_2$, $AlCl_3$ and $CuCl_2$ were acquired from Tianjin Fengchuan Chemical Reagent Co., Ltd. (Tianjin, China). $AgNO_3$ was provided by Shanghai Xunda Fine Chemicals (Shanghai, China). All the experiments were carried out at room temperature with double distilled water (ddH_2O) as the solvent.

2.2 Bacteria preparation and synthesis of CDs

CDs were prepared from *F. nucleatum* cells as a single precursor through a one-step hydrothermal method. The bacterium was incubated on brain heart infusion agar with supplements of 5% goat blood and 10 mg mL^{-1} hemin, and then cultured in a 2.5 L round bottom vertical anaerobic culture bag with the Anaero Pack for 7–10 days in an incubator at 37 °C. After being suspended with 0.85% saline solution, the cell culture was scraped off from the blood agar plate with a triangular coating rod. Subsequently, the bacterial cells collected from 10 blood agar plates were centrifuged with 6000 rpm for 10 min to remove the culture medium. After that, cells were washed with ddH_2O three times through centrifugation at 6000 rpm for 10 minutes each time, and then the cells were resuspended in 35 mL ddH_2O and transferred into a Teflon-lined stainless-steel autoclave (50 mL). After being heated for 24 hours at 180 °C, the light brown solution was collected and then filtered with a syringe filter membrane (0.22 μm). The resultant solution was dried through freeze-drying for 24 hours and the Fn-CDs powder was weighed for further experiments.

2.3 Characterization of Fn-CDs

A PHI5000 Versa probe-II (Shimadzu Co., Japan) was used for X-ray photoelectron spectroscopy (XPS) measurements to examine the elemental components of the prepared Fn-CDs. A Tecnai G2 TF30 S-Twin transmission electron microscope (TEM, FEI Holland) was utilized to investigate the size and morphology of Fn-CDs. The ultraviolet-visible absorption spectra were recorded with a UV-5100H (METASH, Shanghai) spectrophotometer. Both an F-7000 (Hitachi, Japan) fluorescence spectrophotometer and Flex Station 3 (Molecular Devices, USA) multi-mode microplate reader were employed to record the fluorescence spectrum of the obtained Fn-CDs. A Thermo Fisher NICOLET iS10 FTIR spectrophotometer (USA) was employed to acquire the Fourier-transform infrared (FTIR) spectra of Fn-CDs.

2.4 Fluorescence detection of Fe^{3+}

To investigate the selective recognition of the resultant Fn-CDs toward Fe^{3+} ions, various metal cation solutions, including K^+, Fe^{2+}, Ni^{2+}, Zn^{2+}, Mn^{2+}, Ag^+, Cu^{2+}, Ba^{2+}, Li^+, Al^{3+}, Ca^{2+}, Pb^{2+}, and Co^{2+}, were prepared. To 4 mL of ddH_2O, 1 mL (0.7 mg mL^{-1}) of the original solution of Fn-CDs was added and mixed thoroughly for the selective detection assays of Fe^{3+} ions. 50 μL of each metal ion solution was mixed with the same amount of the above Fn-CD solution in each well, and the final concentration

of Fn-CDs and metal ions is 70 μg L^{-1} and 1 mM, respectively. The changes in the PL intensity of Fn-CDs after the addition of metal ions were observed using a microplate reader at an excitation wavelength of 360 nm.

Different concentrations of Fe^{3+} solutions were added to the Fn-CD solutions to evaluate the effects of Fe^{3+} ions on the FL intensity of Fn-CDs under the same experimental conditions described above. The responses of fluorescence intensity to the mixture were collected with a microplate reader at the excitation wavelength of 360 nm. All experiments were conducted at room temperature.

2.5 Cytotoxicity assay of Fn-CDs

The MTS assay method was applied to evaluate the influence of the obtained Fn-CDs on the cell viability of both selected normal cells and normal cells, HeLa cells (cervical cancer cell line, adherent cells), and BEAS-2B (lung normal epithelial cells). The cells were seeded into a 96-well plate at a density of 5000 cells per well in Dulbecco's modified Eagle's medium (DMEM) with supplementation of 10% fetal bovine serum (FBS) and then incubated with Fn-CDs in different concentrations of 12.5 μg, 50 μg, 100 μg and 200 μg at 37 °C under a 5% CO_2 atmosphere for 48 hours. Taxol, an anticancer agent, was used for positive control. After the addition of 20 μL of MTS reagent and 100 μL of medium, the cells were cultured for additional 4 hours. The absorbance of each well was observed at 492 nm on a Multiskan FC (Thermo Fisher, USA).

2.6 Cell imaging

The *in vitro* cell imaging assay was carried out on onion epidermal cells and HeLa cells. Fresh onions were purchased and peeled, the fine layer was selected and cut into small pieces with the width and length of 2 cm, and then immersed in Fn-CD solution for 4 hours. The control was soaked in 0.85% saline. After being washed with ddH_2O twice, the inner epidermal skin of each piece was peeled carefully and placed on the slide, and then observed under a laser confocal scanning microscope.

1 mL of HeLa cells with a density of 50 000 cells per cm^2 was grown in a glass bottom dish containing DMEM with FBS and then incubated at 37 °C under 5% CO_2 atmosphere for 24 hours. Then, 70 μL of Fn-CD solution was added to the cells and the final concentration of Fn-CDs was 56 μg mL^{-1}. After incubation with Fn-CDs for another 24 hours, one group of cells was washed three times with phosphate buffered saline (PBS) to remove the culture medium and the excess Fn-CDs. Finally, the cells in the dish were kept humid in PBS drops and observed under a laser confocal scanning microscope. The other group of cells was observed 48 hours after the addition of Fn-CDs. The cells incubated without Fn-CDs under the same experimental conditions were used as the control.

2.7 Intracellular Fe^{3+} detection

In order to investigate the capacity of Fn-CDs for Fe^{3+} detection in living cells, 1 μL of Fe^{3+} ion stocking solution (100 mmol L^{-1}) was added to HeLa cells incubated with Fn-CDs. The cells were incubated at 37 °C with Fn-CDs (56 μg mL^{-1}) and Fe^{3+} (100 μM) for 4 hours. Then, the cells were washed as described above and observed under a laser confocal scanning microscope.

2.8 *In vivo* fluorescence imaging

6 male Kunming mice with similar size and 14 to 16 g weight were selected to evaluate the feasibility of Fn-CDs for bioimaging *in vivo*. 5 mice were injected intraperitoneally with 10 μL of original solution of Fn-CDs (0.7 mg mL^{-1}) per gram of each mouse. The mouse injected with the same amount of 0.85% saline was used as negative control. The fluorescence images of mice were obtained through an IVIS Lumina Series III imaging system (PerkinElmer, USA). All experiments were carried out in accordance with the relevant laws and institutional guidelines and approved by the Institutional Animal Care and Use Committee at Kunming University of Science and Technology.

3. Results and discussion

3.1 Characterization of Pg-CDs

As seen in Fig. 1, Fn-CDs displayed a nearly spherical shape and a crystalline state. The size distribution of Fn-CDs was within the scope of 2–6 nm with an average size of 4.06 nm in Fig. 1c. The interplanar spacing of 0.15 nm was clearly observed by high-resolution TEM, as shown in Fig. 1b, revealing the graphitic nature of Fn-CDs. The X-ray powder diffraction (XRD) investigation was performed to examine the crystallinity of the solid phase of the resultant Fn-CDs (Fig. 2a). The Fn-CDs showed a broad diffraction peak centered at around 23°, exhibiting a similar graphitic structure as bulk graphite.[26]

The chemical composition and surface structure of the resultant Fn-CDs were studied by X-ray photoelectron spectroscopy (XPS) and Fourier transform infrared (FTIR)

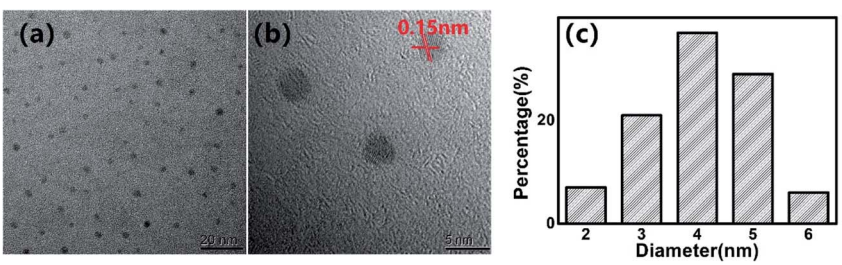

Fig. 1 (a) TEM and (b) HRTEM images of Fn-CDs; (c) size distribution of Fn-CDs.

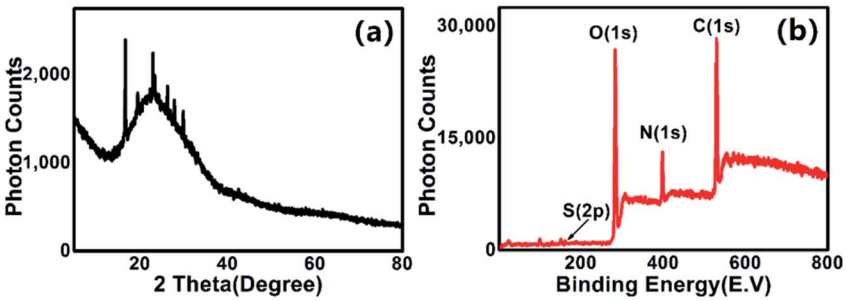

Fig. 2 (a) XRD spectrum of Fn-CDs. (b) XPS spectrum of Fn-CDs.

spectroscopy. The XPS spectra of CDs at low-energy resolution in Fig. 2b revealed four typical peaks at 285.5, 398.1, 532.1 and 160.5 eV, corresponding to O1, N1, C1 and S2p, respectively, indicating that Fn-CDs were mainly composed of carbon, nitrogen, oxygen and sulfur with atomic percentages of 68.10%, 10.18%, 21.38% and 0.34%, respectively.

The high-resolution spectra of C1s shown in Fig. 3a were subdivided into three main peaks approximately at 282.8, 284.0 and 286.0 eV which could be ascribed to C=O, C–H and C–O/C–N bonds, respectively.[26,27] The O1s band in Fig. 3b consisted of two kinds of oxygen species. The peak of 529.6 eV indicated the existence of oxide, while the peak located at 531.6 originated from C=O/OH– groups. Two peaks were seen in the N1s spectrum (Fig. 3c). The peak at 397.8 suggested the existence of N–H groups,[28] while the peak at 399.4 eV was ascribed to the C–N binding group. The S2p spectrum (Fig. 3d) with peaks centered at 161.8 and 165.8 eV revealed the signal of sp^2 sulfur and the existence of –SOH groups, respectively.

The FTIR spectrum in Fig. 4a confirmed the functional groups on the surface of the resultant Fn-CDs. The absorption peaks around 1168 cm^{-1}, 704 cm^{-1} and 1633 cm^{-1} originated from the C=O group, C–S and C=C stretching vibrations, respectively.[29–32] The peaks around 1049 cm^{-1} and 1130 cm^{-1} corresponded to the C=O and C–OH groups, respectively.[26,32] The absorption bands between the regions 3052 and 3624 cm^{-1} arose from the O–H and N–H stretching vibrations.[33–35] The ample chemical groups on the surface may endow the Fn-CDs with distinct optical properties, promoting their application in bioimaging *in vivo*.

3.2 Optical properties of Fn-CDs

The UV-vis absorption spectrum showed a local maximum at 212 nm and a shoulder band at 270 nm, as shown in Fig. 4b, which could be ascribed to the n–σ* absorption of the OH/–NH_2 groups and the n–π* transitions of the C=O groups, respectively.

As seen in the inset in Fig. 4b, the Fn-CDs displayed intense blue fluorescence under 365 nm UV light. As illustrated in Fig. 4c, the FL intensity of Fn-CDs increased when excited at

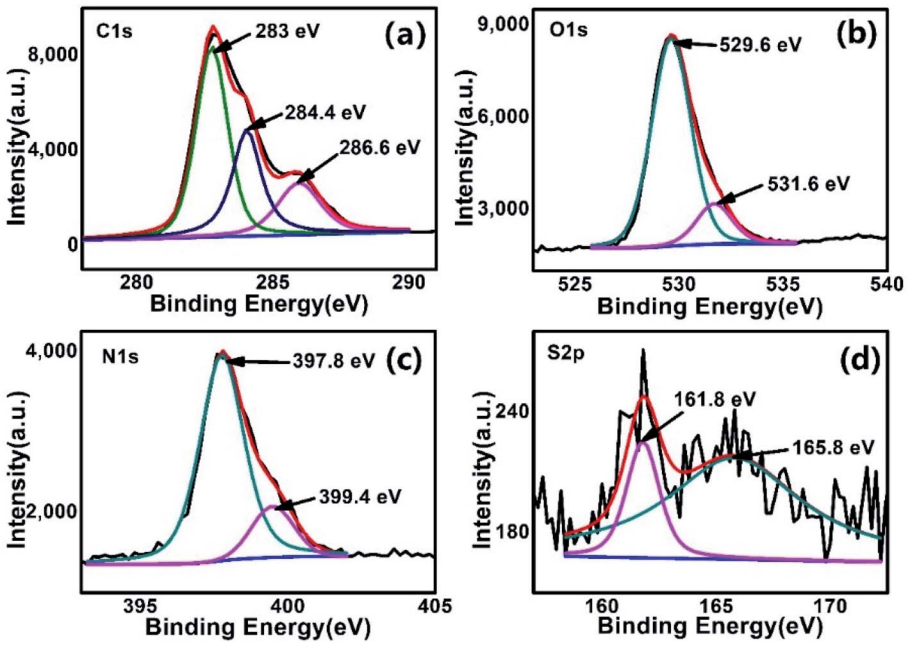

Fig. 3 High-resolution XPS spectra of (a) C1s, (b) O1s, (c) N1s, and (d) S2p of Fn-CDs.

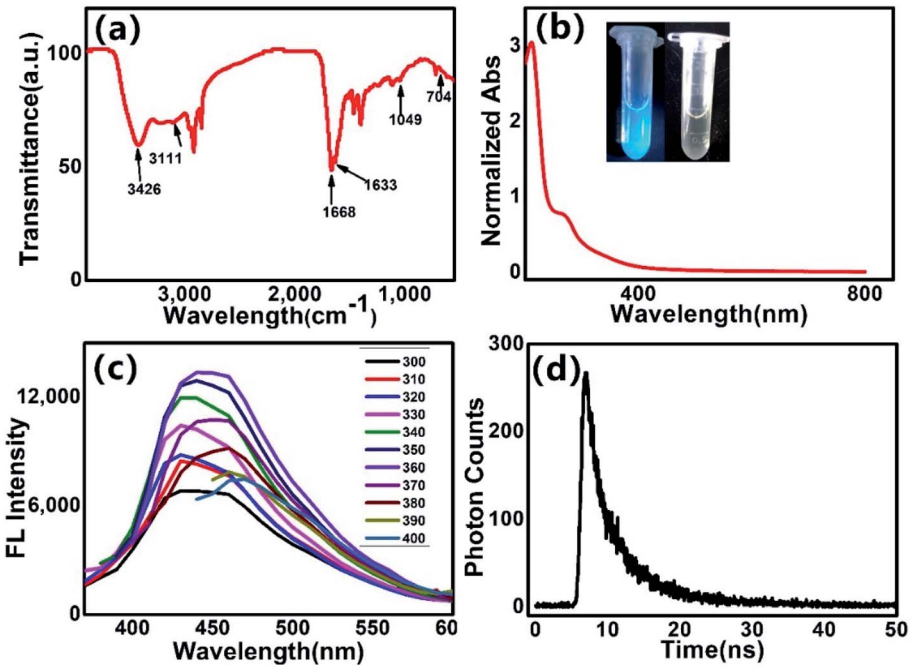

Fig. 4 (a) FTIR spectrum of Fn-CDs; (b) UV-visible absorption spectrum of FN-CDs, inset: photograph of the aqueous Fn-CD solution under irradiation of UV light (right) and daylight (left); (c) emission spectrum of Fn-CDs at different excitation wavelengths; (d) fluorescence decay curve of Fn-CDs.

different wavelengths from 300 to 360 nm in 10 nm increments. The emission peaks showed a clear red shift accompanied by a significant fluorescence intensity decrease, while the excitation wavelength increased stepwise from 360 to 400 nm. The emission peak reached the optimum at 360 nm of excitation wavelength. The emission maxima and bandwidth were distinctly dependent on the excitation wavelength, indicating various radiative sites on the surface of the resultant Fn-CDs, which correlated well with previous studies.[36]

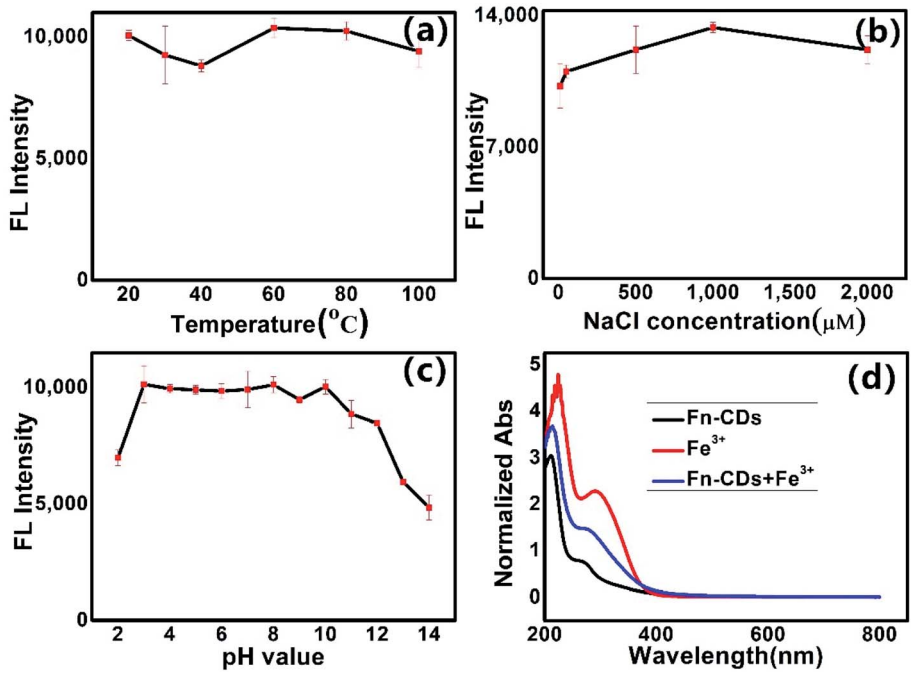

Fig. 5 FL spectra of Fn-CDs at various (a) temperatures; (b) NaCl concentrations; and (c) pH values. (d) UV-visible absorbance spectra of Fn-CDs, Fe^{3+} and Fn-CDs + Fe^{3+}.

The absolute quantum yield was measured as 9.99% using an Edinburgh fluorescence spectrometer (FLS920) with an integrating sphere. The decay curve of Fn-CDs in Fig. 4d revealed its average lifetime of 4.77 ns, as determined by a bi-exponential function with lifetimes of 1.44 ns (16.35%) and 5.42 ns (83.65%) at 360 nm excitation.

Good stability is one of the critical parameters for their application in the biological field. The fluorescence stability of Fn-CDs was evaluated under different conditions including in solutions with pH 2–14, solutions with different ionic concentrations (0 to 2000 μM) and at various temperatures (20 °C to 100 °C) and the changes in the FL intensity were observed. As illustrated in Fig. 5a, the temperature range from 20 to 100 °C did not have a significant effect on the FL intensity. The Fn-CDs displayed high resistance to ionic strength, as shown in Fig. 5b; the FL intensity dropped slightly even in the presence of 2000 μM NaCl. Although the FL intensity declined when pH values were 2 and 14, it remained almost at the same level when the pH value changed from 3 to 10. The above observation revealed that Fn-CDs could maintain their excellent FL performance in a variety of bioenvironments, suggesting that Fn-CDs were suitable for bioimaging under physiological conditions.

3.3 Detection of Fe^{3+}

The impact of fourteen metal ions on the fluorescence intensity of Fn-CDs was recorded to evaluate the feasibility of the probe for Fe^{3+} ions. As shown in Fig. 6a, the fluorescence intensity of Fn-CDs dropped remarkably only after interaction with Fe^{3+} ions, indicating that the resultant Fn-CDs could serve as selective sensor for Fe^{3+} ions. After addition of Fe^{3+} ions with various concentrations ranging from 0 μM to 180 μM, the FL intensity of Fn-CDs decreased gradually (Fig. 6b). Over the range of 20 μM to 180 μM, a good linear relationship between the fluorescence intensity and Fe^{3+} concentration was observed with a correlation coefficient R^2 of 0.98549 (Fig. 6c). F_0 and F were the fluorescence emission peaks before and after addition of Fe^{3+}, respectively. The relationship between the quenching effects and the concentration of Fe^{3+} was well expressed by the following equation:

$$y = 0.00236x + 1.00054$$

The estimated detection limit for Fe^{3+} is 0.82 μM, according to the rule of three times the standard deviation (3σ/slope). Intracellular iron concentration is approximately 0.5 mg mL $^{-1}$ in blood,[37] indicating that Fn-CDs could be used for intracellular Fe^{3+} detection *in vivo*.

The fluorescence quenching mechanism has been investigated extensively. It has been reported that ion exchange or energy transfer between the sensor and ions are two main reasons for fluorescence quenching.[38,39] Fig. 5d shows that the UV absorbance of Fn-CDs in the presence of Fe^{3+} ions increased obviously, suggesting that static quenching may have possibly occurred.[20,33] The red shift of absorbance λ_{max} after addition of Fe^{3+} to Fn-CDs could be related to the interaction between free amino groups on the surface of Fn-CDs and the iron ions.[20]

3.4 Cell cytotoxicity

As seen in Fig. 7a and b, the cell viability of both HeLa cells and BEAS-2B cells incubated with various concentrations of Fn-CDs remained over 80%, much higher than that of same cells treated with Taxol (Fig. 7c and d), the positive control. The prepared Fn-CDs posed low toxicity toward both cancer cells and normal cells at different concentrations, indicating that Fn-CDs possessed excellent biocompatibility and low cytotoxicity.

3.5 Fluorescence bioimaging *in vitro*

From the fluorescence images of onion epidermal cells incubated with Fn-CDs, as shown in Fig. 8a1–a4, we can see that Fn-CDs have penetrated successfully into onion cells, mainly accumulated in the nucleus, some around the cell walls and membranes. Under different excitation light wavelengths of 408, 488 and 555, the onion cells in the presence of Fn-CDs exhibited bright blue, green, and red fluorescence, respectively. No fluorescence was detected in control cells incubated without Fn-CDs (Fig. 8b1–b4).

It has been reported that some CDs could not penetrate into the cells due to certain functional groups, especially hydrophilic groups, such as –OH and –COOH groups on the surface which could confine the CD particles.[40] As shown in Fig. 8b1–b4, the Fn-CDs have crossed the cell membrane successfully and reached the nucleus of the cells. The nucleus and cytoplasm of HeLa cells stained with Fn-CDs displayed bright blue and green light under different excitation wavelengths of 408, 488 and 555, with green being dominant, suggesting that Fn-CDs could serve as a fluorescent probe in the biomedical field.

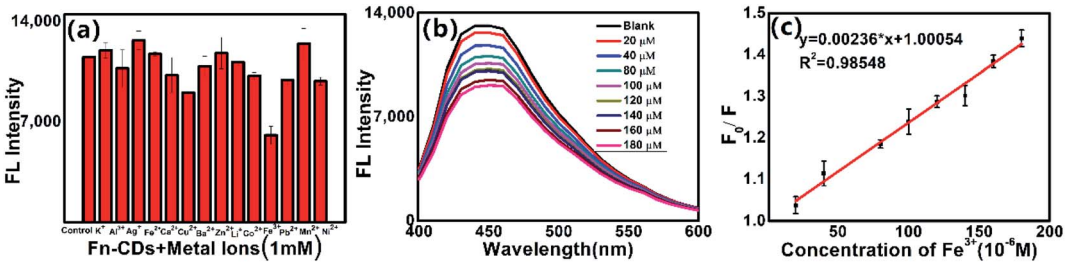

Fig. 6 (a) Effect of 14 metal ions on the FL intensity peaks of Fn-CDs (concentration: Fn-CDs of 40 μg mL^{-1} and metal ion of 1 mM); (b) FL spectrum of Fn-CDs with Fe^{3+} ions (Fe^{3+} concentration: 0, 20, 40, 80, 100, 120, 140, 160, and 180 μM, from top to bottom); (c) linear plot of the relationship between the FL quenching effects and concentration of Fe^{3+} (20 to 180 μM).

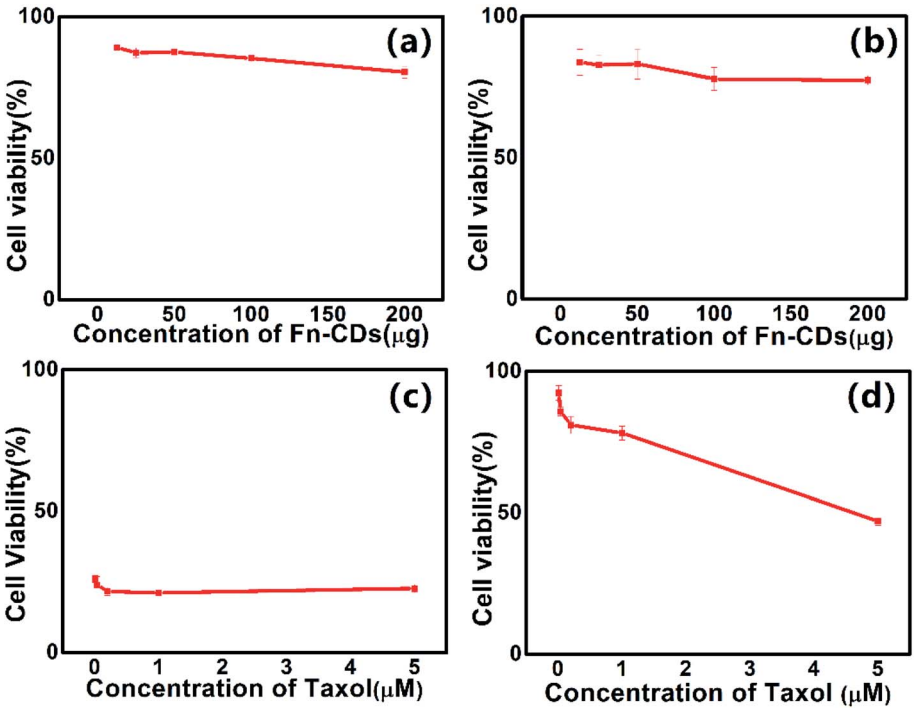

Fig. 7 MTS assay results. (a) Effects of Fn-CDs on HeLa cell viability; (b) effects of Fn-CDs on BEAS-2B cell viability; (c) and (d) positive control. (c) Effects of Taxol on HeLa cell viability. (d) Effects of Taxol on BEAS-2B cells.

The fluorescence could still be observed in the cells after 48 hours of incubation with Fn-CDs (Fig. 9e1–e4). Although the FL intensity appeared weaker, the fluorescence lasted for more than the time required for bioimaging *in vivo*. It was also clearly shown that the number of cells after 48 hours of incubation with Fn-CDs (Fig. 9e1–e4) was more than that observed after incubating for 24 hours with Fn-CDs (Fig. 9b1–b4), confirming that the Fn-CDs did not have negative effects on the growth of cells.

Compared with the cells incubated with only Fn-CDs (Fig. 9c1–c4), the FL intensity of HeLa cells cultured with the addition Fn-CDs and Fe^{3+} reduced noticeably in Fig. 9d1–d4, suggesting that the fluorescence could be quenched in the presence of Fe^{3+} ions in living cells. The concentration of ferric ions in HeLa cells increased after the addition of Fe^{3+}. Therefore, there were extra Fe^{3+} ions in cells which could interact with the chelating groups, such as hydroxyl and amine groups on the

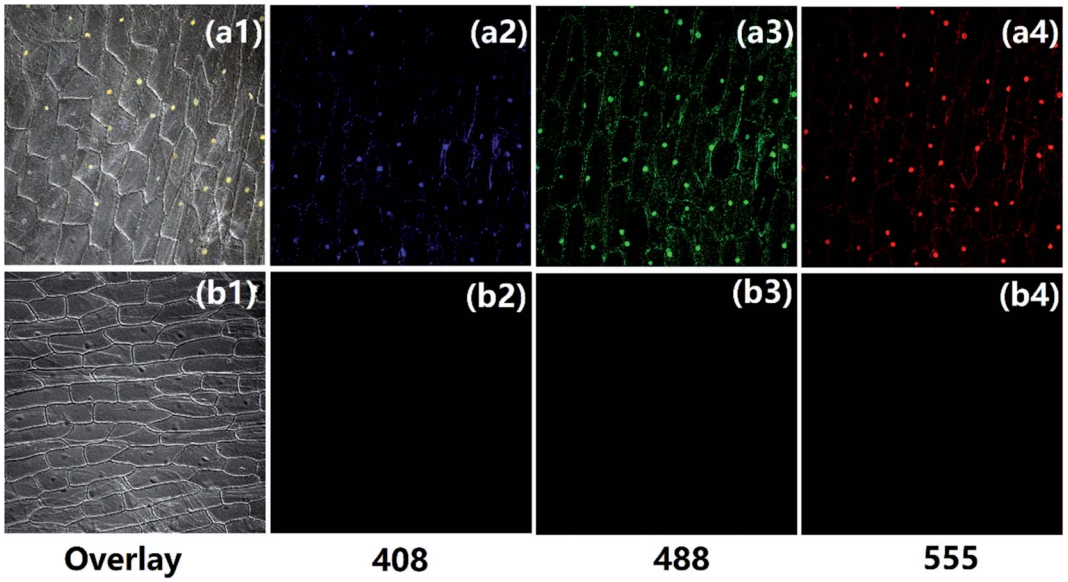

Fig. 8 Confocal images of onion epidermal cells incubated with Fn-CDs (a1–a4) and without Fn-CDs (b1–b4).

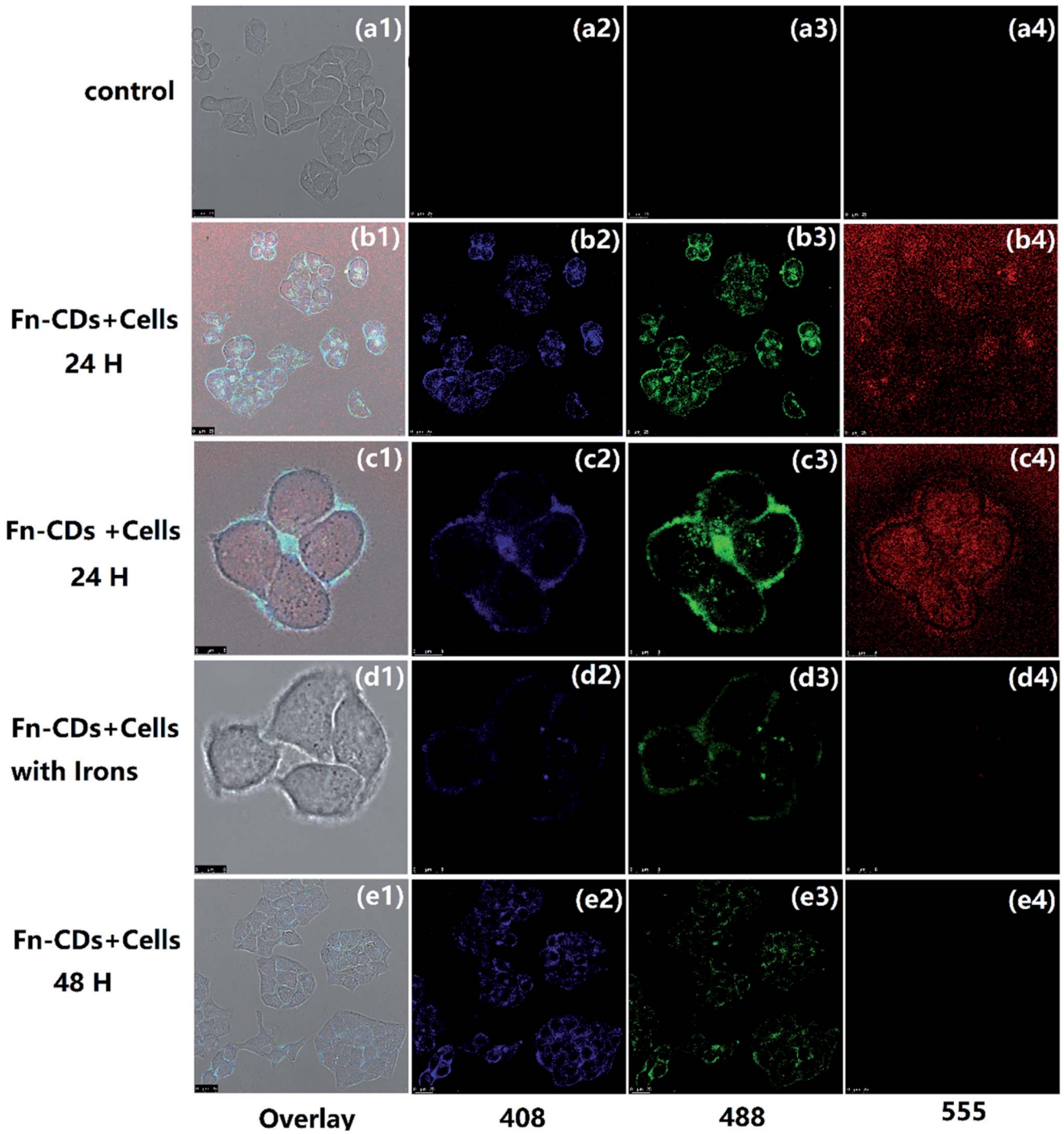

Fig. 9 Confocal images of HeLa cells incubated with Fn-CDs: (b1–b4), (c1–c4) and (e1–e4); without Fn-CDs (a1–a4); with Fn-CDs + Fe^{3+} (concentration of Fn-CDs: 56 μg mL^{-1}; Fe^{3+}: 100 μM).

surface of Fn-CDs, leading to the quenching effects on the fluorescence of Fn-CDs. The above observation demonstrated that the resultant Fn-CDs could be applied as a fluorescent probe for bioimaging and detection of Fe^{3+} *in vivo*.

3.6 Fluorescence bioimaging *in vivo*

Fig. 10 illustrates the fluorescence images of mice taken at different time points after the injection of Fn-CDs. 1 hour after injection, strong fluorescent spots were detected around the injection site and in the stomach. Two hours later, the CDs were found to have spread, and fluorescent signals appeared in the upper parts of mouse, probably around the location of lungs and heart. The fluorescence was found accumulated on the lower part of mouse by 5 hours, to the area of small intestine. Later on, the FL intensity decreased gradually, demonstrating that the CDs may have entered into the blood circulation and

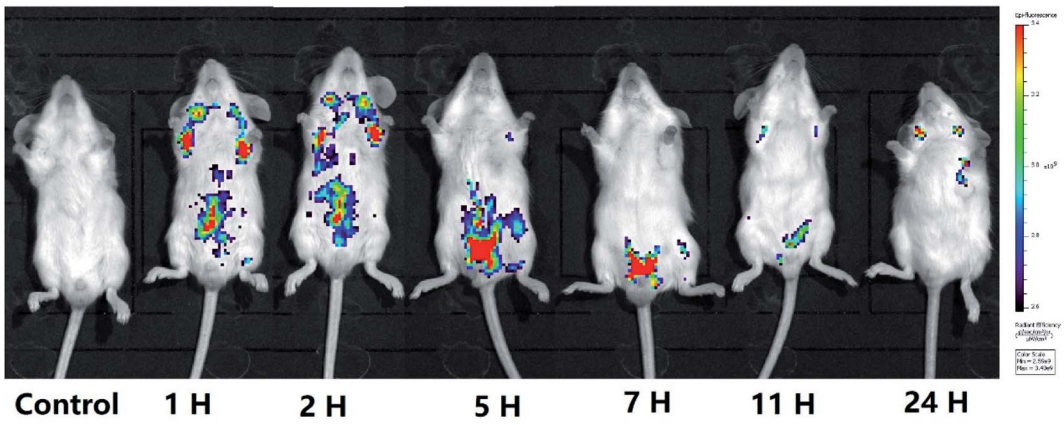

Fig. 10 *In vivo* fluorescence imaging of male Kunming mice at different treated times with Fn-CDs (10 μL g^{-1}, 0.7 mg mL^{-1}).

carried to other parts of the body. We speculated that the Fn-CDs could probably have penetrated the blood–brain barrier (BBB) to the brain. The Fn-CDs could be excreted through digestion as no signal was detected 24 hours after injection, indicating that the Fn-CDs have been cleared out of the body within a short time.

4. Conclusions

In this study, for the first time, an anaerobic bacterium *F. nucleatum* was utilized to synthesize CDs through a hydrothermal method. TEM, XRD, FTIR, XPS, fluorescence and UV-vis absorption spectroscopy were employed to characterize the properties of the resultant Fn-CDs. The Fn-CDs exhibited high stability, long-term bioimaging and excellent biocompatibility. Most significantly, the prepared Fn-CDs were selectively sensitive to the presence of Fe^{3+} and could serve as an intracellular Fe^{3+} biosensor. In addition, the Fn-CDs also have been successfully applied for imaging in plant cells, HeLa cells, and in mice as well, suggesting their great potential applications in *in vitro* and *in vivo* bioimaging. Whether the Fn-CDs can cross the blood–brain barrier (BBB) and internalize the brain requires further investigation.

Author contributions

Lijuan Liu: Writing – original draft. Shengting Zhang: Writing – review & editing. Xiaodan Zheng: Formal analysis. Hongmei Li: Methodology. Qi Chen: Software. Kunhao Qin: Resources. Yafang Ding: Data curation. Yunlin Wei: Supervision.

Conflicts of interest

The authors declare that they have no conflict of interest.

Acknowledgements

We are grateful for the financial support of this work provided by National Natural Science Foundation of China (31960232) and Scientific Research Fund of Yunnan Education Department (2021J0653).

References

1 C. Dias, N. Vasimalai, P. Sárria Marisa, I. Pinheiro, V. Vilas-Boas, J. Peixoto and B. Espina, Biocompatibility and Bioimaging Potential of Fruit-Based Carbon Dots, *Nanomaterials*, 2019, **9**(2), 199.
2 T. Zhou, Z. Huang, F. Wan and Y. Sun, Carbon quantum dots-stabilized Pickering emulsion to prepare NIR light-responsive PLGA drug delivery system, *Mater. Today Commun.*, 2020, **23**, 100951.
3 A. Nair, J. T. Haponiuk, S. Thomas and S. Gopi, Natural carbon-based quantum dots and their applications in drug delivery: A review, *Biomed. Pharmacother.*, 2020, **132**, 110834.
4 M. Ashrafizadeh, R. Mohammadinejad, S. K. Kailasa, Z. Ahmadi, E. G. Afshar and A. Pardakhty, Carbon dots as versatile nanoarchitectures for the treatment of neurological disorders and their theranostic applications: A review, *Adv. Colloid Interface Sci.*, 2020, **278**, 102123.
5 H. Li, X. Yan, D. Kong, R. Jin, C. Sun, D. Du, Y. Lin and G. Lu, Recent advances in carbon dots for bioimaging applications, *Nanoscale Horiz.*, 2020, **5**, 218–234.
6 Z. Qu, L. Liu, S. Tiedong, J. Hou, Y. Sun, M. Yu, Y. Diao, S. Lu, W. Zhao and L. Wang, Synthesis of bifunctional carbon quantum dots for bioimaging and anti-inflammation, *Nanotechnology*, 2020, **31**, 175102.
7 D. Li, X. Yuan, C. Li, Y. Luo and Z. Jiang, A novel fluorescence aptamer biosensor for trace Pb(II) based on gold-doped carbon dots and DNAzyme synergetic catalytic amplification, *J. Lumin.*, 2020, **221**, 117056.
8 F. Xu, H. Tang, J. Yu and J. Ge, A Cu^{2+}-assisted fluorescence switch biosensor for detecting of coenzyme A employing nitrogen-doped carbon dots, *Talanta*, 2021, **224**, 121838.
9 X. Wei, L. Li, J. Liu, L. Yu, H. Li, F. Cheng, X. Yi, J. He and B. Li, Green Synthesis of Fluorescent Carbon Dots from *Gynostemma* for Bioimaging and Antioxidant in Zebrafish, *ACS Appl. Mater. Interfaces*, 2019, **11**, 9832–9840.

10 J. Shi, G. Ni, J. Tu, X. Jin and J. Peng, Green synthesis of fluorescent carbon dots for sensitive detection of Fe^{2+} and hydrogen peroxide, *J. Nanopart. Res.*, 2017, **19**, 209.
11 G. G. Naik, M. B. Alam, V. Pandey, D. Mohapatra, P. K. Dubey, A. S. Parmar and A. N. Sahu, Multi-Functional Carbon Dots from an Ayurvedic Medicinal Plant for Cancer Cell Bioimaging Applications, *J. Fluoresc.*, 2020, **30**, 407–418.
12 S. Wang, W. Sun, D.-s. Yang and F. Yang, Soybean-derived blue photoluminescent carbon dots, *Beilstein J. Nanotechnol.*, 2020, **11**, 606–619.
13 Q. Huang, Q. Li, Y. Chen, L. Tong, X. Lin, J. Zhu and Q. Tong, High quantum yield nitrogen-doped carbon dots: green synthesis and application as "off-on" fluorescent sensors for the determination of Fe^{3+} and adenosine triphosphate in biological samples, *Sens. Actuators, B*, 2018, **276**, 82–88.
14 K. Dehvari, K. Y. Liu, P.-J. Tseng, G. Gedda, W. M. Girma and J.-Y. Chang, Sonochemical-assisted green synthesis of nitrogen-doped carbon dots from crab shell as targeted nanoprobes for cell imaging, *J. Taiwan Inst. Chem. Eng.*, 2019, **95**, 495–503.
15 R. Atchudan, T. N. Jebakumar Immanuel Edison, M. Shanmugam, S. Perumal, T. Somanathan and Y. R. Lee, Sustainable synthesis of carbon quantum dots from banana peel waste using hydrothermal process for *in vivo* bioimaging, *Phys. E*, 2021, **126**, 114417.
16 Y. Sun, S. Zheng, L. Liu, Y. Kong, A. Zhang, K. Xu and C. Han, The Cost-Effective Preparation of Green Fluorescent Carbon Dots for Bioimaging and Enhanced Intracellular Drug Delivery, *Nanoscale Res. Lett.*, 2020, **15**, 55.
17 S. K. Kailasa, S. Ha, S. H. Baek, L. M. T. Phan, S. Kim, K. Kwak and T. J. Park, Tuning of carbon dots emission color for sensing of Fe^{3+} ion and bioimaging applications, *Mater. Sci. Eng., C*, 2019, **98**, 834–842.
18 V. N. Mehta, S. Jha, H. Basu, R. K. Singhal and S. K. Kailasa, One-step hydrothermal approach to fabricate carbon dots from apple juice for imaging of mycobacterium and fungal cells, *Sens. Actuators, B*, 2015, **213**, 434–443.
19 P. Liyanage, R. Graham, R. Pandey, C. Chusuei, K. Mintz, Y. Zhou, J. Harper, W. Wu, A. Wikramanayake, S. Vanni and R. Leblanc, Carbon Nitride Dots: A Selective Bioimaging Nanomaterial, *Bioconjugate Chem.*, 2018, **30**, 111–123.
20 L. Liu, K. Qin, S. Yin, X. Zheng, H. Li, H. Yan, P. Song, X. Ji, Q. Zhang, Y. Wei and L. Zhao, Bifunctional Carbon Dots Derived From an Anaerobic Bacterium of Porphyromonas gingivalis for Selective Detection of Fe^{3+} and Bioimaging, *Photochem. Photobiol.*, 2020, DOI: 10.1111/php.13360.
21 A. U. Steinbicker and M. U. Muckenthaler, Out of balance – systemic iron homeostasis in iron-related disorders, *Nutrients*, 2013, **5**, 3034–3061.
22 E. C. Theil and D. J. Goss, Living with Iron (and Oxygen): Questions and Answers about Iron Homeostasis, *Chem. Rev.*, 2009, **109**, 4568–4579.
23 V. K. Gupta, N. Mergu and L. K. Kumawat, A new multifunctional rhodamine-derived probe for colorimetric sensing of Cu(II) and Al(III) and fluorometric sensing of Fe(III) in aqueous media, *Sens. Actuators, B*, 2016, **223**, 101–113.
24 L. Guo, T. Tang, L. Hu, M. Yang and X. Chen, Fluorescence assay of Fe(III) in human serum samples based on pH dependent silver nanoclusters, *Sens. Actuators, B*, 2017, **241**, 773–778.
25 A. Harrandah, S. Chukkapalli, A. Progulske-Fox, W. Dunn, K. Lakshmyya and E. Chan, Abstract 5139: *F. nucleatum* induces invasive phenotypes in oral cancer cells *in vitro*, *Cancer Res.*, 2018, **78**, 5139.
26 B. Wu, R. Zhu, M. Wang, P. Liang, Y. Qian and S. Wang, Fluorescent carbon dots from antineoplastic drug etoposide for bioimaging *in vitro* and *in vivo*, *J. Mater. Chem. B*, 2017, **5**, 7796–7800.
27 Y. Meng, Y. Jiao, Y. Zhang, Y. Li, Y. Gao, W. Lu, Y. Liu, S. Shuang and C. Dong, Multi-sensing function integrated nitrogen-doped fluorescent carbon dots as the platform toward multi-mode detection and bioimaging, *Talanta*, 2020, **210**, 120653.
28 Y. Tu, S. Wang, X. Yuan, Y. Wei, K. Qin, Q. Zhang, X. Chen and X. Ji, A novel fluorescent nitrogen, phosphorus-doped carbon dots derived from *Ganoderma lucidum* for bioimaging and high selective two nitrophenols detection, *Dyes Pigm.*, 2020, **178**, 108316.
29 Z. Qu, L. Liu, T. Sun, J. Hou, Y. Sun, M. Yu, Y. Diao, S. Lu, W. Zhao and L. Wang, Synthesis of bifunctional carbon quantum dots for bioimaging and anti-inflammation, *Nanotechnology*, 2020, **31**, 175102.
30 X.-W. Hua, Y.-W. Bao, H.-Y. Wang, Z. Chen and F.-G. Wu, Bacteria-derived fluorescent carbon dots for microbial live/dead differentiation, *Nanoscale*, 2017, **9**, 2150–2161.
31 F. Lin, C. Li and Z. Chen, Bacteria-Derived Carbon Dots Inhibit Biofilm Formation of *Escherichia coli* without Affecting Cell Growth, *Front. Microbiol.*, 2018, **9**, 259.
32 F. Huo, W. Liang, Y. Tang, W. Zhang, X. Liu, D. Pei, H. Wang, W. Jia, P. Jia and F. Yang, Full-color carbon dots with multiple red-emission tuning: on/off sensors, *in vitro* and *in vivo* multicolor bioimaging, *J. Mater. Sci.*, 2019, **54**, 6815–6825.
33 C. Shi, H. Qi, R. Ma, Z. Sun, L. Xiao, G. Wei, Z. Huang, S. Liu, J. Li, M. Dong, J. Fan and Z. Guo, N,S-Self-doped carbon quantum dots from fungus fibers for sensing tetracyclines and for bioimaging cancer cells, *Mater. Sci. Eng., C*, 2019, **105**, 110132.
34 X. Liang, H. Liu, Y. Du, W. Li, M. Wang, B. Ge and L. Zhao, Terbium functionalized covalent organic framework for selective and sensitive detection of LVX based on fluorescence enhancement, *Colloids Surf., A*, 2020, **606**, 125429.
35 B. S. B. Kasibabu, S. L. D'Souza, S. Jha, R. K. Singhal, H. Basu and S. K. Kailasa, One-step synthesis of fluorescent carbon dots for imaging bacterial and fungal cells, *Anal. Methods*, 2015, **7**, 2373–2378.
36 H. Liao, C. Jiang, W. Liu, J. M. Vera, O. D. Seni, K. Demera, C. Yu and M. Tan, Fluorescent Nanoparticles from Several Commercial Beverages: Their Properties and Potential

Application for Bioimaging, *J. Agric. Food Chem.*, 2015, **63**, 8527–8533.

37 A. U. M. Steinbicker and M. U. Muckenthaler, Out of Balance—Systemic Iron Homeostasis in Iron-Related Disorders, *Nutrients*, 2013, **5**, 3034–3061.

38 S. Bian, C. Shen, H. Hua, L. Zhou, H. Zhu, F. Xi, J. Liu and X. Dong, One-pot synthesis of sulfur-doped graphene quantum dots as a novel fluorescent probe for highly selective and sensitive detection of lead(II), *RSC Adv.*, 2016, **6**, 69977–69983.

39 Q. Xu, P. Pu, J. Zhao, C. Dong, C. Gao, Y. Chen, J. Chen, Y. Liu and H. Zhou, Preparation of highly photoluminescent sulfur-doped carbon dots for Fe(III) detection, *J. Mater. Chem. A*, 2015, **3**, 542–546.

40 J. Wang, M. Xu, D. Wang, Z. Li, F. L. Primo, A. C. Tedesco and H. Bi, Copper-Doped Carbon Dots for Optical Bioimaging and Photodynamic Therapy, *Inorg. Chem.*, 2019, **58**, 13394–13402.